A 50μm Pitch, 1120-Channel, 20kHz Frame Rate Microelectrode Array for Slice Recording

Ben Johnson*, Shane T. Peace†, Thomas A. Cleland‡, and Alyosha Molnar*
*School of Electrical and Computer Engineering
†Department of Neurobiology and Behavior
‡Department of Psychology
Cornell University
Ithaca, NY 14853, USA

***Abstract*— We present a 1,120 channel active microelectrode array with 50μm pitch recording sites for direct recording of neural slices. Every sensor site has a frontend low noise amplifier and photopixel for correlating optical stimulus with electrical activity. The frontend is AC-coupled and achieves area-efficiency by integrating the large input capacitor and recording electrode directly over the circuitry in conjunction with a single T-capacitor feedback network. Degraded PSRR (63dB) and CMRR (21dB) from the single feedback network are overcome by utilizing a virtual shared reference, improving rejection to 84dB and 66dB, respectively. Despite a small area, the frontend amplifier has an input-referred noise of 4.3μVrms with tunable high- and low-pass corners with very little variation from site-to-site. Experiments from a transgenic mouse olfactory bulb slice are shown. The array was implemented in a standard 180nm CMOS process.**

I. Introduction

In order to study the microcircuitry of neural tissue, neurophysiologists utilize microelectrode arrays (MEAs) to simultaneously acquire electric field activity across relatively large areas of neural tissue. In dense neural tissue, like the cortex, isolation of single cell activity is extremely difficult with a single recording site, meaning densely-packed, multisite recording arrays are required for cell localization and sorting (Fig. 1). Increasing the number of recording electrodes allows for more simultaneous single cell recordings as well as spatially broad analysis of local field potentials (LFPs) that provide insight into how and under what conditions neuronal ensembles synchronize activity.

Most commercially available MEAs are fabricated on passive substrates and use off-substrate amplifiers, with routing constraints typically limiting them to 256 electrodes or less. CMOS MEAs can drastically increase the spatial density and number of electrodes by locally multiplexing channels onto fewer wires. MEAs intended for slice recording (as in this work) should have a recording area large enough to accommodate an entire slice (>1mm^2 for mouse hippocampal and olfactory bulb slices) while having an electrode pitch fine enough to sample single action potentials with multiple electrodes (<100μm) [1]. MEAs must also have low noise signal conditioning (<5μVrms) and an adequate sampling rate and tuning range for action potentials and LFPs (>10kHz). These constraints conflict with each other such that state-of-the-art CMOS arrays typically have focused on meeting

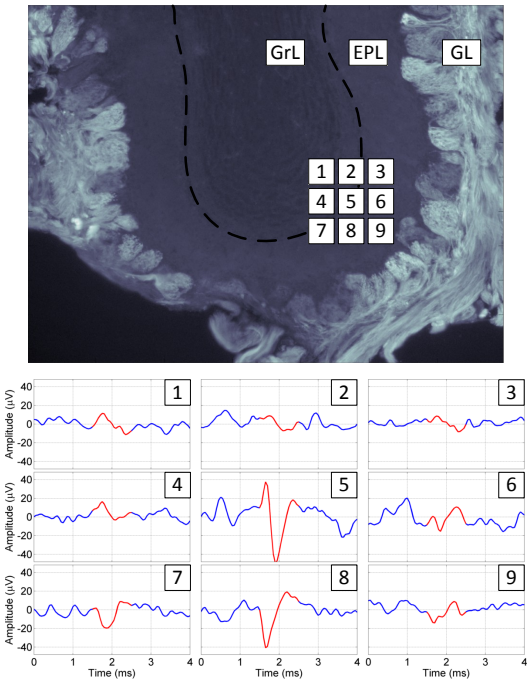

Fig. 1. Image of mouse olfactory bulb slice and simultaneous planar MEA recording. The glomerular layer (GL) circuitry includes the axonal arbors of primary olfactory sensory neurons that express ChR2-YFP. Spiking activity and LFP oscillications are primarily recorded from the external plexiform layer (EPL).

only a subset of these challenges. Arrays with pixel-level amplification that achieve a fine pitch and large electrode count can have slow sample rates and significant noise [2]. Arrays with column-level amplification achieve superior noise performance by using larger amplifiers at the expense of increasing sensor pitch [3] or reducing overall number of simultaneous recording sites [4].

While MEAs provide massively parallel, high-fidelity recording of the output of neuronal assemblies, precise control over the network input is also desired [1]. Electrical stimulation at the microscale is difficult as it creates large recording artifacts and can cause toxic redox reactions [5]. Chemical stimulation can avoid artifacts, but is typically spatially nonspecific. Optical stimulation, however, can be spatially and temporally precise, cell-specific, and contact-free. In visual neuroscience, computer-generated patterns of

978-1-4799-1471-5/13/$31.00 ©2013 IEEE

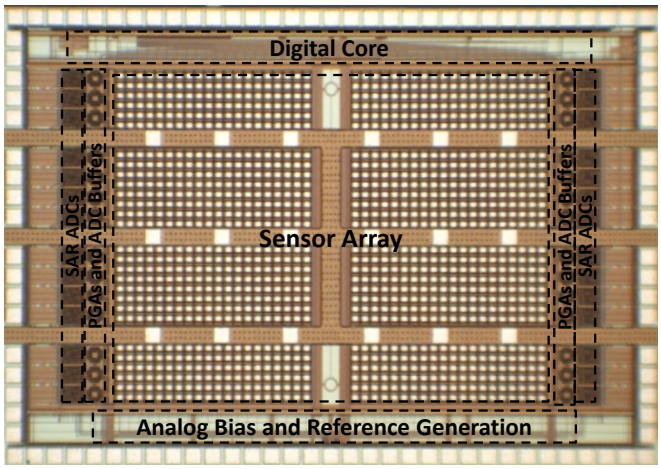

Fig. 2. Microphotograph of the fabricated array. The size of the sensor area is 2.2 x 1.7 mm^2.

light can be used to stimulate retinal photoreceptors while electrically recording activity from the ganglion cells, the retinal output. Similarly, optogenetics allows researchers to create light-sensitive cells in other biological systems to understand the way they process information [6]. For example, neuronal cells expressing the light-reactive protein channelrhodopsin-2 (ChR2) can be excited optically (Fig. 1). While passive MEAs built on transparent substrates allow for visual correlation of electrode location, tissue, and stimulus, active MEAs on silicon substrates severely limit this capability.

Therefore, the aim of this work is provide researchers with an MEA that overcomes the limitations of both traditional passive and active MEAs for slice research. This work records biopotentials across the tissue sample at 1,120 locations at a rate of 20kHz with a spatial resolution of 50μm for sampling action potentials and a large active area to sample coherent LFPs (Fig. 2). Despite an area-constrained design, the frontend amplifier achieves low input-referred noise of 4.3μVrms with capacitive feedback for precise gain and tunable low- and high-pass filtering. Additionally, because optogenetics is a rapidly growing technique in neurophysiological research, the MEA also has photodiodes adjacent to each recording electrode, enabling the reliable correlation of recorded electrophysiological data with the recorded spatiotemporal patterns of optical stimulation.

II. MEA Design

A. System Overview

The system was implemented in a standard 180nm 1P6M CMOS process with 4μm-thick top metal with an active area of 2.2 x 1.7 mm^2 (Fig. 2). Fig. 3 illustrates the overall architecture of the system, comprising 28 rows with 40 recording sites each. Each channel contains a low-noise amplifier, tunable low- and high-pass filters, and a buffer. A 6-bit, 40 count gray code generated in the digital core selects between electrodes in each row to activate each site's buffer. Each row includes a switched-capacitor programmable gain amplifier (PGA) with 4 gain settings (18 dB, 21.5 dB, 24 dB, or 26 dB), a unity

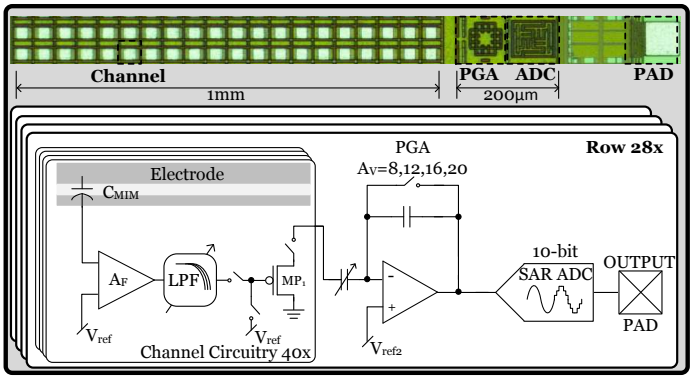

Fig. 3. Block diagram of the row architecture.

gain buffer, and a 10-bit SAR ADC. The PGA implements correlated double sampling by amplifying the difference between the electrode signal and the frontend reference through the channel buffer. Correlated double sampling removes the variable offsets of every source follower in the row circuit, reduces the amount of output swing required by the PGA, and enables control of the PGA output DC level.

The dynamic range of extracellular neural signals from brain slices typically does not exceed 45dB, therefore the ADC uses 10 bit resolution to ensure that the quantization noise of the ADC is well below the noise floor of the recorded neural activity and frontend circuitry while providing margin for unexpectedly large input signals such as stimulation or perfusion artifacts. The SAR ADC uses a 5b/5b split capacitor array to reduce area and loading on the ADC buffer. Each ADC is operated at 800kS/s, effectively sampling each electrode at 20kHz and yielding a total aggregate data rate of 224Mb/s from 28 output pads.

B. Unit-Sensor Design

A key challenge for high-density, robust recording is achieving low-noise and high gain with area-efficient circuits [7]. Local filtering and amplification are necessary at each electrode to limit the thermal noise from the electrode interface (typically the dominant noise source for MEAs) and prevent aliasing under rapid multiplexing of signals. High gain and low output impedance at the pixel-level are desired to relax noise requirements of subsequent signal conditioning stages and to reduce crosstalk and EMI pickup [8]. Traditional neural amplifiers use capacitive coupling to block low frequency electrochemical offsets and capacitive feedback to accurately set the gain across channels [3]. The gain is set by the ratio of the input capacitor to the feedback capacitor. The feedback capacitor value is typically set by parasitics and matching (roughly 150fF), resulting in very large areas for sufficient gain (40dB). Therefore, this work uses a capacitive T-network to decouple the gain from the maximum capacitor ratio, allowing a closed-loop gain of 41.2dB with ratios less than 17:1 (Fig. 4). The T-network creates an effective gain feedback capacitance (C_{gain}) of

$$C_{gain} = \frac{C_2 \cdot C_4}{C_2 + C_3 + C_4} \quad (1)$$

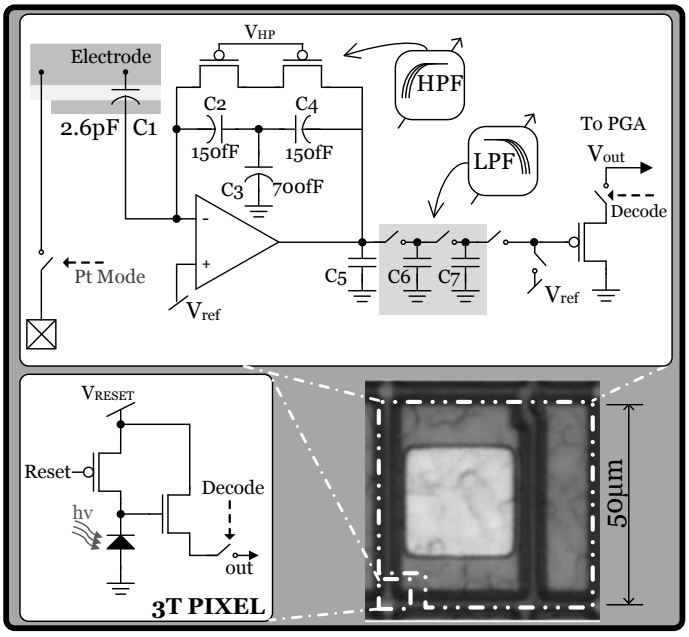

Fig. 4. Unit-sensor with frontend amplifier and photopixel.

where the closed loop gain of the amplifier is C_1 / C_{gain}. C_{gain} is now 22.5fF, which is smaller than the minimum size MIM capacitor without sacrificing matching.

While decreasing the size of the input capacitor can save significant area, it has a few caveats. Ensuring C_1 is much larger than the feedback network and the input capacitance of the amplifier ($C_{in,amp}$) mitigates most of the issues. The input-referred noise of the open-loop amplifier ($V^2_{n,amp}$) sees a different transfer function than the input signal, and is related to the input of the system as

$$V^2_{n,fdbk} = \left(\frac{C_1 + C_{ff} + C_{in,amp}}{C_1}\right)^2 \cdot V^2_{n,amp}, \qquad (2)$$

where

$$C_{ff} = \frac{C_2 \cdot (C_3 + C_4)}{C_2 + C_3 + C_4}. \qquad (3)$$

C_{ff} is the feed-forward capacitance of the T-network as seen from the input of the amplifier. The input pair is large to suppress flicker noise; however, increasing its area increases the noise gain.

Note that equation 2 neglects kT/C noise from the feedback network, which is dominant at low frequencies due to a small C_{gain}. Once again, a large input capacitor (high gain) will mitigate noise injected by the feedback impedance. kT/C noise can also be shifted by the high-pass corner (ω_{HP} = 1 / $R_{eff}C_{gain}$). The high-pass corner is controlled by a PFET in triode with a large incremental resistance (R_{eff}). The main purpose of the high-pass corner is to keep low frequency artifacts from saturating the system. The low-pass corner of the amplifier is also adjustable to selectively filter for LFP or spikes, optimizing the array for different experimental conditions. The low-pass corner is set by a switched-capacitor filter on the output of the amplifier ($\omega_{LP} \approx f_{sw}C_6$ / C_7). Since the corner is determined by a ratio of local capacitors and a switching frequency, the corner is robust against mismatch.

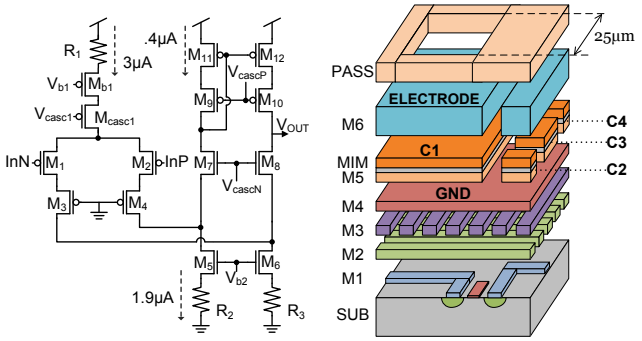

Fig. 5. Transistor-level schematic of frontend amplifier and illustration of the metal stack configuration used to form electrode interface.

Fig. 5 shows the transistor-level schematic of the amplifier. The amplifier uses a low-power folded-cascode topology with source degeneration resistors to reduce noise and improve matching [9]. Since there is no matching feedback network for the reference, the amplifier is more susceptible to power supply fluctuations coupling through the C_{GS} of M_1. We use principal component analysis (PCA) to remove common-mode signals, improving PSRR. PCA is effective because the array records from several sites simultaneously distributed across a large spatial area, meaning that the recorded neural signals are not likely to be correlated. Noise from the differential pair biasing cannot be removed through PCA, so R_1 was inserted to degenerate noise from M_{b1}.

The electrode circuitry was designed to interface directly to neural tissue in an aqueous environment. The interface electrode is formed by a 25μm by 25μm passivation opening over the top plate of the input MIM capacitor (Fig. 5). M4 was used exclusively as a ground plane in the sensor area to provide additional electrical, ionic and light shielding. One corner is unshielded to allow light to pass to the photodiode. A switch connects the top plate of the input MIM capacitor to an externally controlled voltage to enable the controlled platinization of electrodes.

III. Measurement Results

While significant variation in high-pass corner frequencies was expected across the chip, direct measurements shown in Fig. 6 indicate that the variation (σ = 0.8Hz, roughly 10%) is sufficiently small for biopotential applications. Variation in the midband gain (with gain loss from the buffer) and the low-pass corner were measured to be 0.6% and 1.2%, respectively, demonstrating good matching across the array. The frontend input-referred noise was 4.3μVrms (measured from 20Hz - 50kHz) from a 1.8V, 3.8μA supply, corresponding to a noise efficiency factor (NEF) of about 3.4 for a bandwidth of 20Hz to 9kHz, competitive with state-of-the-art neural preamplifiers with much larger areas [3]. The measured average PSRR and CMRR across the array was 63dB and 21dB, respectively. After performing PCA, the average PSRR and CMRR were improved to 84dB and 66dB. The backend signal conditioning achieved an ENOB of 8.2 bits at 800kS/s, demonstrating a sufficient SNR for neural recording. The power consumption of all analog frontends, PGAs, and ADCs was 14.1mW,

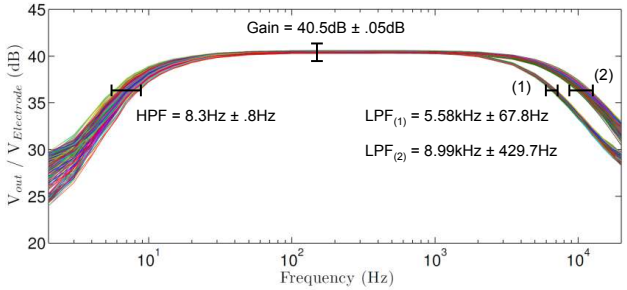

Fig. 6. Measured transfer function of the frontend amplifier with variation measured across the array (N = 1120). $LPF_{(1)}$ has the switched-capacitor filter engaged, reducing the variation of the low-pass corner frequency.

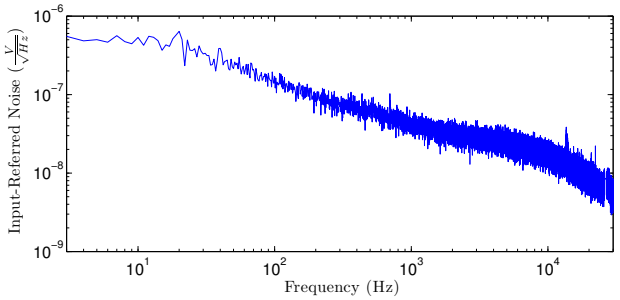

Fig. 7. Measured input-referred noise of the frontend amplifier.

corresponding to 12.6μW per channel.

Post-processing the system for neural recordings involved defining a well around the sensor array with silicone, and then encapsulating the bondwires with epoxy. Since the exposed metal is aluminum, which corrodes easily in saline and is cytotoxic, the electrodes were electroplated with platinum black. Platinum is nontoxic and decreases electrode impedance, hence reducing the noise contributions from the electrode interface. Electroplating was performed by filling the well with platinizing solution, applying a positive potential to a platinum counter-electrode, and holding the electrodes at a fixed potential by activating internal platinization circuitry.

The functionality of the system was verified by recording spiking and LFP activity from a 300μm-thick mouse olfactory bulb slice. The tissue was horizontally sliced with a vibrating microtome and then placed in oxygenated 34C aCSF. Fig. 8 shows recording of endogenous neural activity recorded from three electrodes. Due to the fine pitch of the array, single action potentials can be spatially oversampled.

An iPad with Retina display approximately 1m above the array was used to generate test inputs for the photopixels. A 20mm, f1.8 Sigma lens was used to focus images from the screen onto the sensor array. Fig. 9 demonstrates that the sensor array can be used to determine whether optical stimuli are focused and capturing video.

IV. Conclusion

This work presented a 1,120-channel electrode array for neural slice recording. Despite a small area (50μm by 50μm), each channel had a power-efficient, low-noise amplifier (4.3μVrms) and photopixel for optical sensing. The array demonstrated good matching across channels and was used to record neural activity from a neural slice.

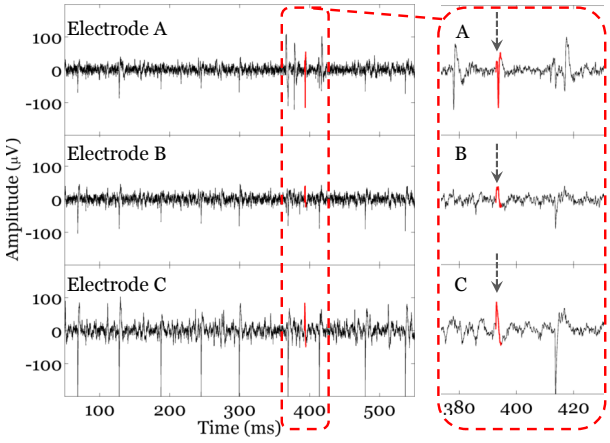

Fig. 8. Spiking activity recorded from a mouse olfactory bulb slice placed directly on the array.

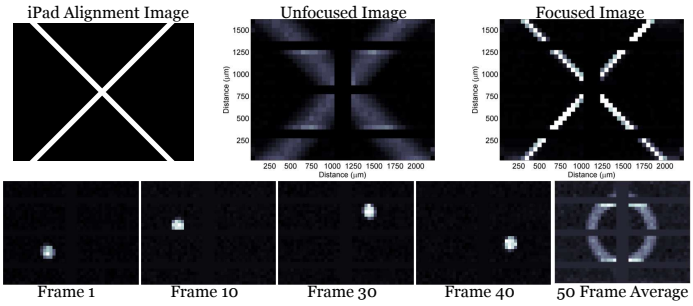

Fig. 9. Alignment images generated by an iPad and images captured by the sensor array used to focus the stimulus (top). Video of a rotating dot captured at 16fps (bottom).

References

[1] H. Buzsaki, "Large-Scale Recording of Neuronal Ensembles," *Nat Neurosci*, vol. 7, no. 5, pp. 446-451, May 2004.

[2] A. Lambacher, V. Vitzthum, R. Zeitler, M. Eickenscheidt, B. Eversmann, R. Thewes, and P. Fromherz, "Identifying Firing Mammalian Neurons in Networks with High-Resolution Multi-Transistor Array (MTA)," *Appl. Phys. A*, vol. 102, pp. 1-11, Jan. 2011.

[3] J. Aziz, K. Abdelhalim, R. Shulyzki, R. Genov, B. Bardakjian, M. Derchansky, D. Serletis and P. Carlen, "256-Channel Neural Recording and Delta Compression Microsystem With 3D Electrodes," *IEEE J. Solid-State Circuits*, vol. 44, pp. 995-1005, Mar. 2009.

[4] U. Frey, F. Heer, R. Pedron, M. Ballini, J. Mueller, D. Bakkum, S. Hafizovic, F. Faraci, F. Greve, K. Kirstein and A. Hierlemann, "Switch-Matrix-Based High Density Microelectrode Array in CMOS Technology," *IEEE J. Solid-State Circuits*, vol. 45, pp. 476-482, Feb. 2010.

[5] K. Y. Kown, B. Sirowatka, W. Li, and A. Weber, "Opto-μECoG array: Transparent μECoG electrode array and integrated LEDs for optogenetics," in *Proc. IEEE BioCAS Conf.*, 2012, pp. 164-167.

[6] E. Boyden, F. Zhang, E. Bamberg, G. Nagel and K. Deisseroth, "Millisecond-timescale, genetically targeted optical control of neural activity," *Nat Neurosci*, vol. 8, no. 9, pp. 1263-1268, Aug. 2005.

[7] M. Elzeftawi, S. Beach, L. Wang, and L. Theogarajan, "A 1.3μW 0.0075mm^2 Neural Amplifier and Capacitor-Integrated Electrodes for High Density Neural Implant Recording," in *Proc. IEEE BioCAS Conf.*, 2012, pp. 236-239.

[8] C. M. Lopez, A. Andrei, S. Mitra, M. Welkenhuysen, W. Eberle, C. Bartic, R. Puers, R. F. Yazicioglu, and G. Gielen, "An Implantable 455-Active-Electrode 52-Channel CMOS Neural Probe," *ISSCC Dig. Tech. Papers*, pp. 288-289, Feb. 2013.

[9] W. Wattanapanitch, M. Fee and R. Sarpeshkar, "An Energy-Efficient Micropower Neural Recording Amplifier," *IEEE Trans. Biomed. Circuits Syst.*, vol. 1, pp. 136-147, Jun. 2007.